JOURNAL OF MATERIALS SCIENCE 20 (1985) 3957–3966

A high-resolution transmission electron microscope study of a zinc oxide varistor

HIDEYUKI KANAI, MOTOMASA IMAI, TAKASHI TAKAHASHI
Toshiba Corporation Research and Development Centre, Kawasaki, Kanagawa 210, Japan

Investigations were made of varistor microstructure, the morphology of Bi_2O_3 at multiple ZnO grain junctions, Bi_2O_3/ZnO grain boundaries and ZnO/ZnO grain boundaries (especially whether Bi_2O_3 is present or not at the ZnO/ZnO grain boundary) by means of high-resolution transmission electron microscopy and X-ray microanalysis in the scanning transmission electron microscope. Bi_2O_3 at multiple ZnO grain junctions consists of small particles of 0.1 μm in diameter, and they are vitrified to some extent. It is suggested that bismuth ions dissolve into ZnO grains over a 30 nm range from a Bi_2O_3/ZnO grain boundary; however, there is no bismuth at ZnO/ZnO grain boundaries.

1. Introduction

The zinc oxide varistor is an electronic ceramics device which exhibits highly non-linear current–voltage characteristics [1–3]. It has been used widely as a small-surge absorber to protect electrical circuits from surge, and as a lightning arrester for high voltage transmission lines. It is produced by sintering a mixture of ZnO with additives of Bi_2O_3, CoO, MnO and other oxides at 1100 to 1300° C. The microstructure consists of ZnO grains, a Bi_2O_3 phase which surrounds ZnO grains, and $Zn_{2.33}Sb_{0.67}O_4$ spinels [4]. The highly non-linear characteristics are attributed to the three-dimensional structure of the ZnO grain, which is an n-type semiconductor, and the Bi_2O_3 layer which has a high resistance [2–6]. Many conduction mechanisms of the varistor have been proposed on the basis of its microstructure [7–12].

There are several studies on varistor microstructure [13–15]. Clarke [13] has suggested that Bi_2O_3 is present only at multiple ZnO grain junctions as an amorphous phase, and that the majority of the ZnO/ZnO grain boundaries are devoid of any intergranular phase. Kingery *et al.* [14] have suggested that there is a region of bismuth segregation over the distance from a ZnO/ZnO grain boundary to 10 nm inside the boundary, independent of the presence of an intergranular phase. Therefore, there are continuous regions of substantially enriched bismuth concentration at all grain boundaries. However, it is not clear how the Bi_2O_3 exists over a range of 10 nm, and there is little information on the lattice distortion of ZnO in the vicinity of the grain boundary where bismuth concentration exists.

As mentioned above, there are several unknown points concerning the ZnO/ZnO grain boundary. It is very important for understanding the conducting mechanism and the degradation mechanism to clarify the ZnO/ZnO grain boundary.

To clarify these points, it is necessary to observe the varistor microstructure more minutely down to the level of atomic configuration. It is very helpful to use a high-resolution image and an optical diffraction method [16], which gives us information on the true image and on lattice distortion at the grain boundaries. In conventional electron diffraction, the dimension of the area selected is of the order of 1 to 2 μm due to objective lens aberration. Thus it is very difficult to extract information from a small region. However, the area selected can be reduced down to about 1 nm by the optical dif-

0022–2461/85 $03.00 + .12

fraction method. Thus this technique is expected to be very helpful for the investigation of the ultrastructure.

This paper presents new information on the morphology of Bi_2O_3 at multiple ZnO grain junctions, Bi_2O_3/ZnO grain boundaries and ZnO/ZnO grain boundaries. In particular, an investigation was made to determine whether bismuth ions are present or not at ZnO/ZnO grain boundaries. This investigation was carried out by high-resolution transmission electron microscopy (HR–TEM), optical diffraction, and scanning transmission electron microscope (STEM) analysis.

2. Experimental details

Specimens were prepared from powders of ZnO, Bi_2O_3, CoO, MnO and other oxides. These powders were mixed sufficiently and pressure moulding was carried out. The resultant pellet was sintered for 2 h at 1250° C and heat treated for 1 h.

The non-linear characteristics of the varistor are generally evaluated by the following equation:

$$I = \left(\frac{V}{C}\right)^{\alpha}$$

wherein V is the applied voltage, I is the resultant current flowing through the varistor and α is a non-linear coefficient. The non-linear coefficient of our sample was 100, and its voltage–current non-linear characteristics were excellent.

Thin foil specimens for HR–TEM and STEM were prepared from a thin section by argon ion thinning. Microscopic observation was carried out at 200 kV. An energy-dispersive X-ray spectrometer (EDX) was used for X-ray microanalysis in STEM. The approximate detection limit of EDX is 10^{-18} to 10^{-19} g.

An optical diffraction pattern was obtained using a standard diffractometer. The film which was obtained at a magnification of 300 000, was used as a sample for optical diffraction. A rectangular aperture (3 mm × 2 mm) was used to select the area. The area selection corresponds to about 7 nm × 10 nm on the specimen.

3. Results

3.1. The morphology of Bi_2O_3 at multiple ZnO grain junctions

An electron micrograph of Bi_2O_3 at multiple ZnO grain junctions is shown in Fig. 1. It consists of small particles of Bi_2O_3 of 0.1 μm diameter. Diffraction patterns from two different regions at this multiple ZnO grain junctions are shown in Fig. 1. There are mostly γ-Bi_2O_3 and a small amount of β-Bi_2O_3 and non-stoichiometric $Bi_2O_{2.33}$ in Region (i), but no β-Bi_2O_3 at Region (ii). This fact shows that the Bi_2O_3 phases, which constitute multiple ZnO grain junctions, are different at locations in a junction.

TABLE I Interplanar spacing of $Bi_2O_{2.33}$

Diffraction plane	d_{ASTM} (nm)	d_{obs} (nm)
004	0.8775	0.835
006	0.585	0.581
008	0.4388	0.437
00$\underline{10}$	0.351	0.349

Non-stoichiometric $Bi_2O_{2.33}$ [17] has not been reported in a varistor. Table I shows the interplanar spacings of $Bi_2O_{2.33}$. They were measured from the diffraction pattern. They were increased by a small amount compared with spacings described in ASTM 27–51.

A ring-shaped diffraction pattern is seen dimly. This fact suggests two possibilities. That is, Bi_2O_3 in Region (i) contains a small amount of fine particles or coexists with glassy phase. This leads to the conclusion that Bi_2O_3 is partially amorphous.

3.2. Bi_2O_3/ZnO grain boundaries

Fig. 2 shows an electron micrograph at a Bi_2O_3/ZnO grain boundary. The (1 0 0) lattice fringes are seen to be continuous right up to the Bi_2O_3/ZnO grain boundary. The interplanar spacing was measured to be 0.280 nm from the diffraction pattern. The image of the grain boundary joining the two arrows in Fig. 2 is faint, and contrast is brighter than that in the ZnO and Bi_2O_3 grains. In order to investigate the grain boundary and its close vicinity more minutely, an optical diffraction method was used. A typical optical diffraction pattern, from the rectangular area corresponding to Region A1 in Fig. 3, is shown in Fig. 4. A ring-shaped diffraction pattern, as well as a (1 0 0) diffraction spot is seen in Fig. 4. It is inferred that the Bi_2O_3/ZnO grain boundary consists of an amorphous region of about 3 nm width, which is partially crystalline. The width was measured from the micrograph in Fig. 2. Furthermore, (1 0 0) interplanar spacings at Regions A1, A2

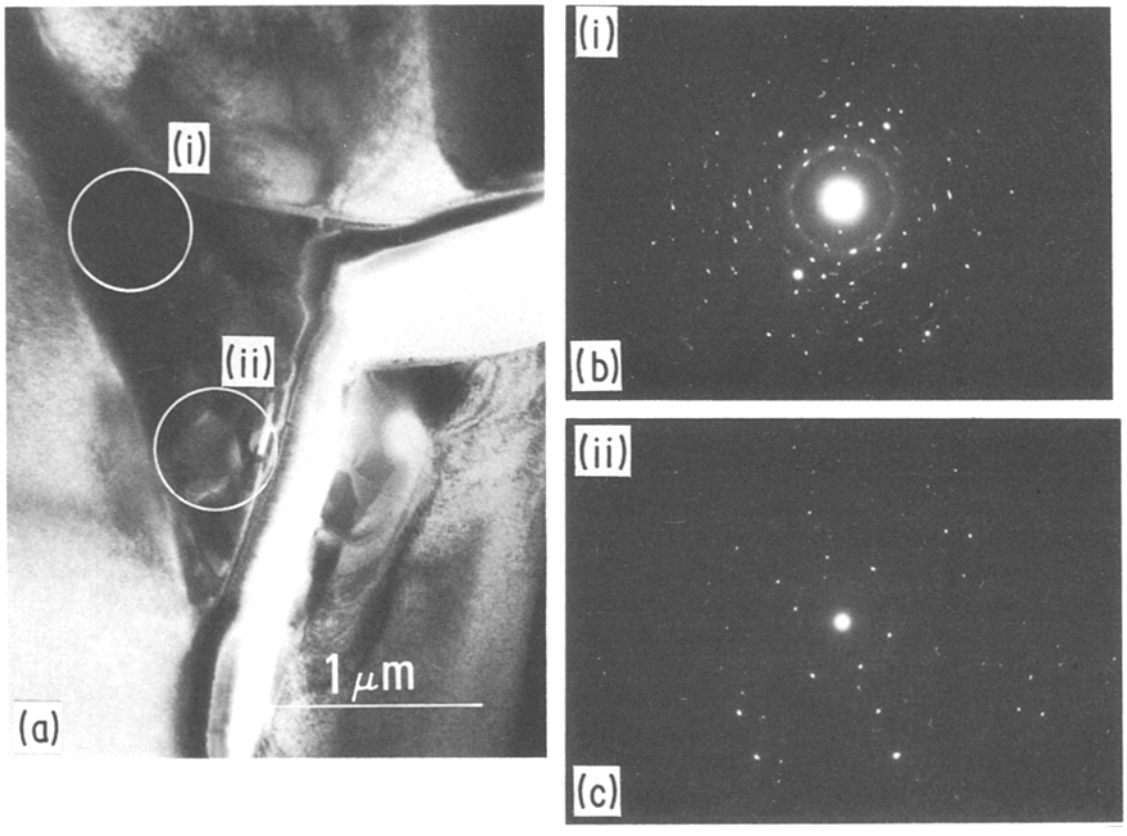

Figure 1 (a) Transmission electron micrograph of Bi_2O_3 at multiple ZnO grain junctions, (b) and (c) diffraction patterns from Regions (i) and (ii).

and A3 were measured by using optical diffraction patterns. The result is given in Fig. 5.

In Region A1 adjacent to the Bi_2O_3/ZnO grain boundary, which is 3 nm from the boundary, the spacing is expanded by about 1.2% from the standard spacing. However, it decreased with distance from the boundary and it became constant at a point 30 nm from the boundary.

3.3. ZnO/ZnO grain boundaries

Fig. 6 shows the lattice-fringe image of a ZnO/ZnO grain junction. The boundary lies along a line joining the two arrows. This photograph indicates an important fact: that is, the (0 0 2) lattice fringes (d = 0.260 nm) and the (1 0 1) lattice fringes (d = 0.248 nm) are seen to be continuous and straight right up to the grain boundary. It is widely believed that there is a secondary phase between adjacent ZnO grains, but the secondary phase cannot be discerned in Fig. 6. Only a disordered layer exists, which is less than 1 to 2 nm in width. However, terminating fringes in adjacent grains, which are seen in the boundary, seem to be joined coherently across the disordered layer. Optical diffraction patterns from Regions B1, B2, B3, B4, B5 and B6 of Fig. 7 were used in obtaining Fig. 8 which shows (0 0 2) and (1 0 0) interplanar spacings from adjacent grains. Both spacings do not change over a wide range, from the vicinity of the ZnO/ZnO grain boundary to the ZnO grain inside.

4. Discussion

4.1. Bi_2O_3/ZnO grain boundaries

Two reasons are considered for the lattice expansion of ZnO, which was observed at the Bi_2O_3/ZnO grain boundary. One is the dissolution of bismuth ions into the ZnO lattice, due to the relatively large Bi^{3+} radius. The other is lattice strain caused by mismatch at the Bi_2O_3/ZnO grain boundary.

Fig. 9 shows the results of STEM analysis at

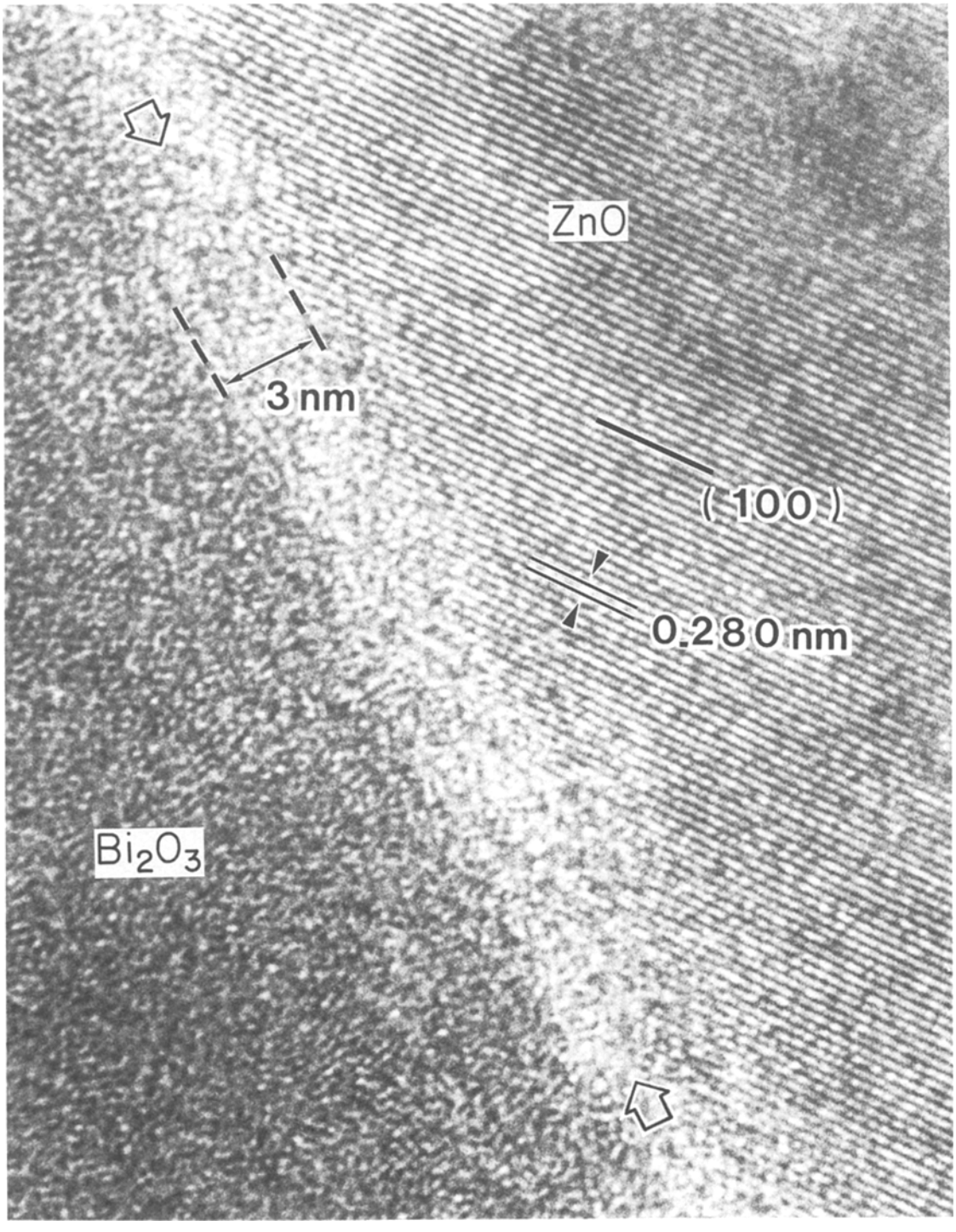

Figure 2 HR-TEM photograph showing Bi_2O_3/ZnO grain boundary and (1 0 0) lattice fringe image.

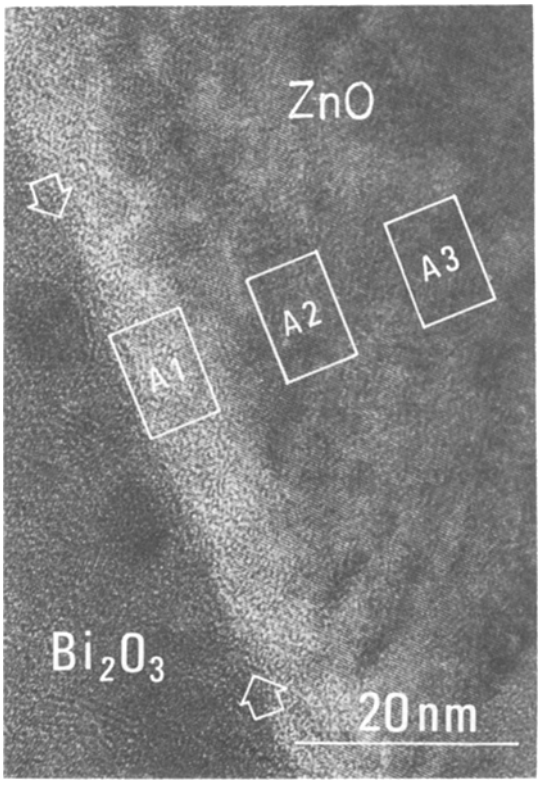

Figure 3 HR–TEM photograph showing Bi_2O_3/ZnO grain boundary. Rectangular areas indicate selected areas for optical diffraction.

the regions near the multiple ZnO grain junctions. Bismuth ions were detected at the Bi_2O_3/ZnO grain boundary (Point 1), and a small amount of bismuth ions was detected even 19 nm inside the ZnO grain (Point 2). However, bismuth ions were not detected at a point 65 nm inside from the boundary. These results show that there is a distribution of bismuth concentration in the vicinity of the Bi_2O_3/ZnO grain boundary, and it decreases with distance from the boundary.

The effect of a mismatch at the Bi_2O_3/ZnO grain boundary on the lattice expansion of ZnO is not clear, but it is difficult to imagine that the mismatch could cause lattice expansion over such a wide range of 18 nm. Thus, it is considered that the reason for the lattice expansion is bismuth ion dissolution into the ZnO lattice.

4.2. ZnO/ZnO grain boundaries

As shown in Fig. 6, no secondary phase is discerned, though there is a disordered layer

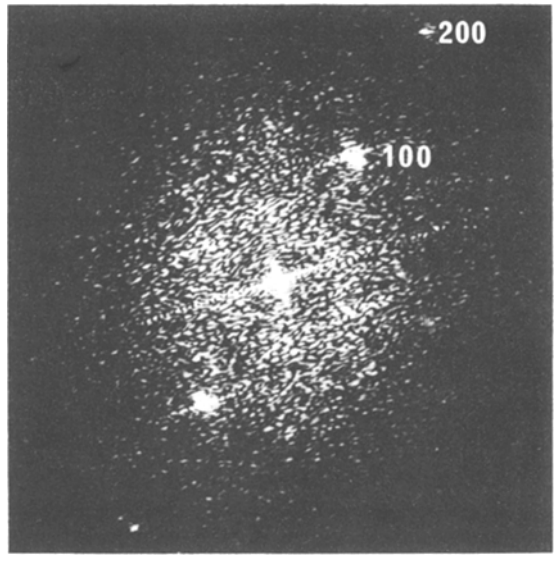

Figure 4 Optical diffraction pattern from Region A1 in Fig. 3. The ring-shaped diffraction pattern shows the existence of an amorphous region.

which is less than 1 to 2 nm in width. If there was a Bi_2O_3 layer at the ZnO/ZnO grain boundary or dissolution of bismuth ions near the ZnO/ZnO grain boundary, the expansion of the ZnO lattice (which is observed in the vicinity of the Bi_2O_3/ZnO grain boundary) could be measured. Clearly, this is not the case. Both spacings do not change over a wide range from the vicinity of the ZnO/ZnO grain boundary to the inside of the ZnO grain.

Fig. 10 shows the results of STEM analysis at the ZnO/ZnO grain boundary. Bismuth ions were not detected at the boundary. The approximate detection limit of EDX is 10^{-18} to 10^{-19} g, so the minimum number of bismuth atoms needed to be detected is 2.9×10^2. Because the electron probe of STEM is 10 to 15 nm in

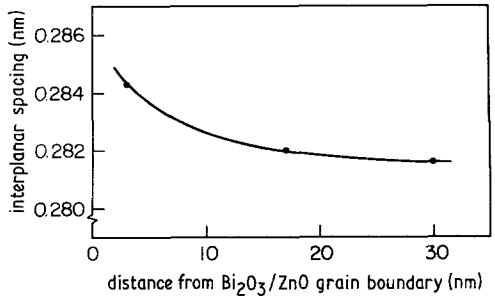

Figure 5 Variation of (1 0 0) interplanar spacing near Bi_2O_3/ZnO grain boundary.

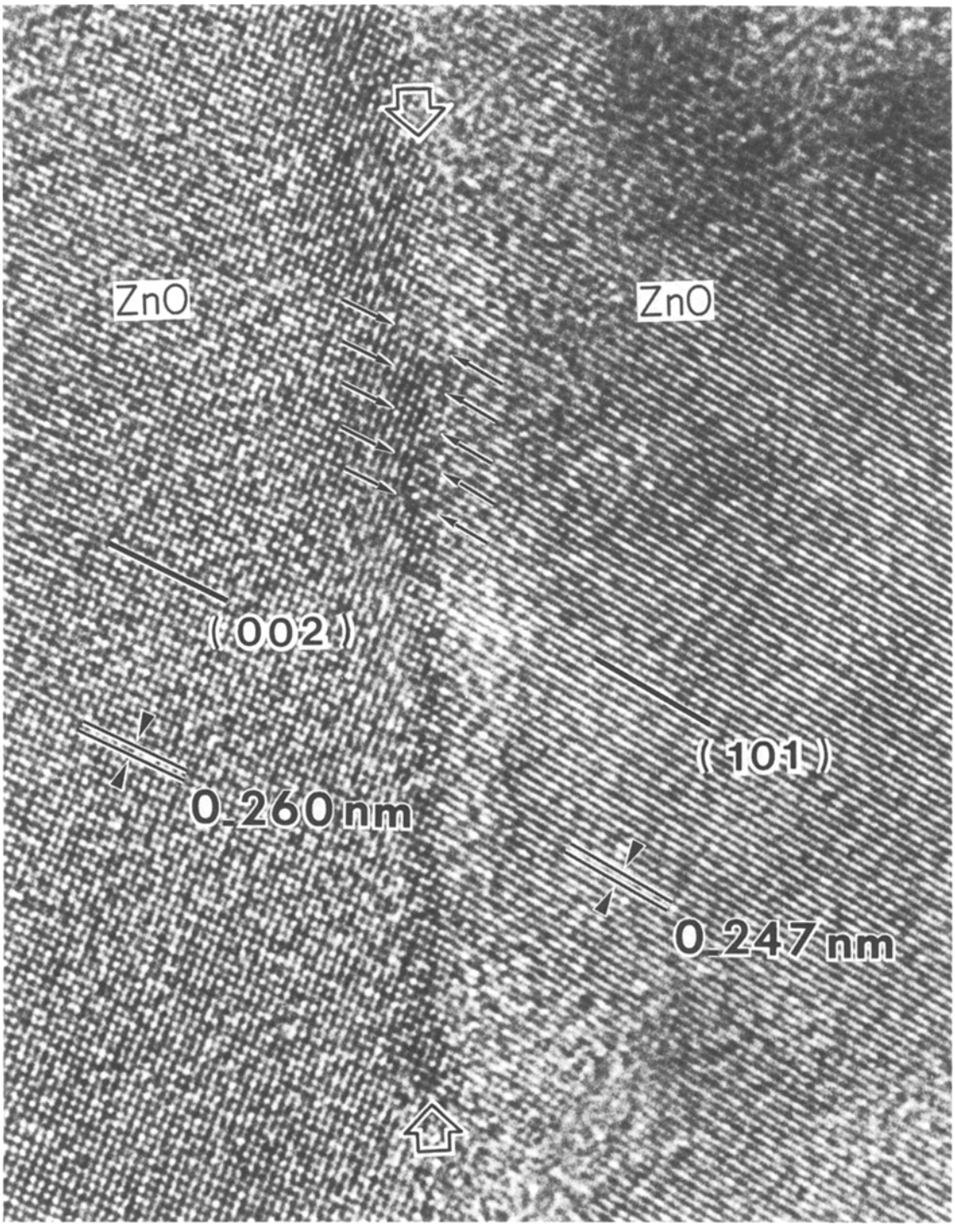

Figure 6 HR–TEM photograph showing ZnO/ZnO grain boundary and (1 0 1) and (0 0 2) lattice fringe images.

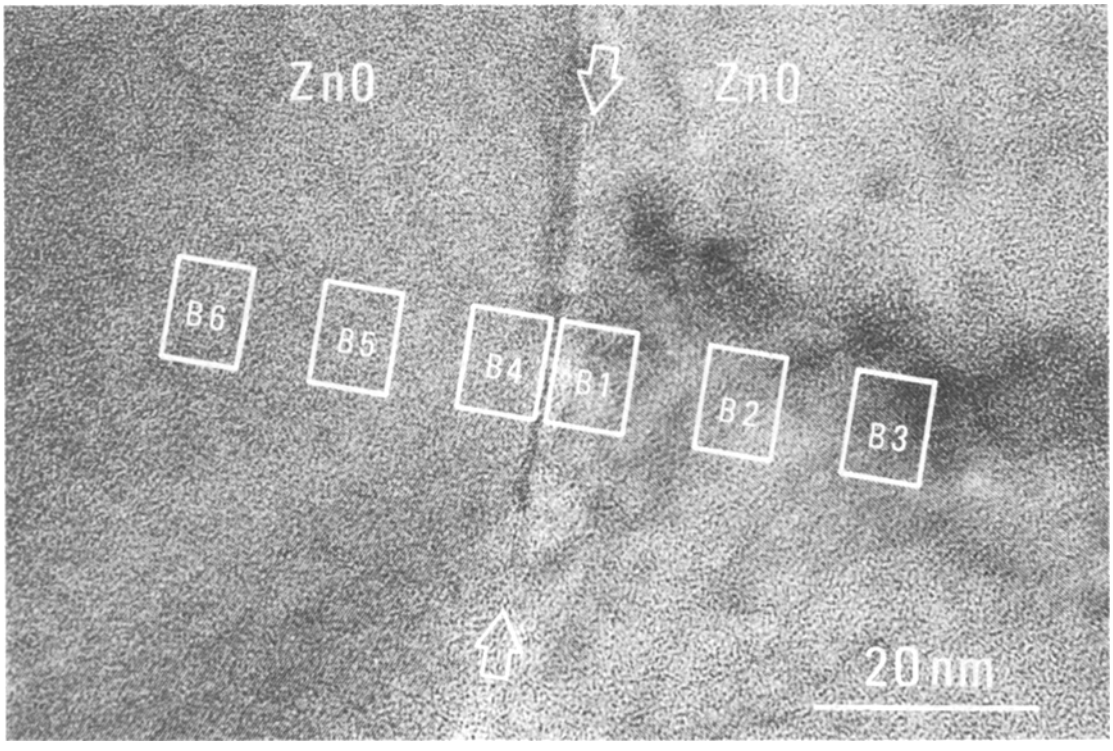

Figure 7 HR–TEM photograph showing ZnO/ZnO grain boundary. Rectangular areas indicate selected areas for optical diffraction.

diameter, assuming that the detection region is 10 nm × 10 nm × 50 nm (sample thickness is deduced to be at least 50 nm), this region contains almost 1.1×10^5 zinc atoms. According to Kingery *et al.* [14] there is an enriched bismuth concentration at the ZnO/ZnO grain boundary. On the basis of this report, supposing the bismuth concentration is 0.03 (= Bi/Zn) on an average in the present detection region, this region would contain 6.3×10^3 bismuth atoms. Therefore, if the bismuth concentration reported [14] exists, bismuth should be detected. However, no indication of bismuth could be obtained from electron diffraction, HR–TEM or STEM analysis at any ZnO/ZnO grain boundaries.

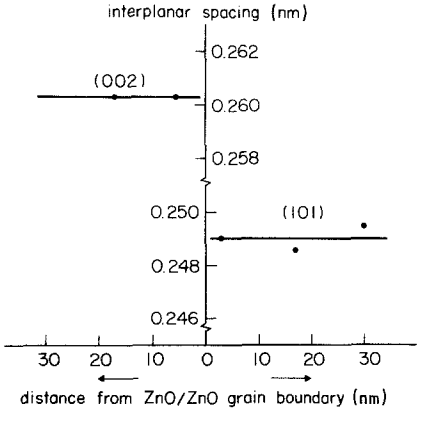

Figure 8 Variation of (1 0 1) and (0 0 2) interplanar spacings near the ZnO/ZnO grain boundary in Fig. 7.

Therefore, we conclude that there is no secondary phase and no bismuth at ZnO/ZnO grain boundaries. Even if bismuth exists there, it is considered that the quantity is less than 10^{-19} g.

5. Summary

The emphasis in this paper is placed on the grain boundary structure, especially whether or not bismuth ions are present at the ZnO/ZnO grain boundary. The microstructure was also clarified: that is, only a disordered layer of about 1 nm in width existed at the ZnO/ZnO grain boundary, and no secondary phase such as a Bi_2O_3 layer nor bismuth ion dissolution into the ZnO lattice could be found.

This conclusion leads us to the following suggestion. In order to cause the non-linear current–voltage characteristic, it is not always

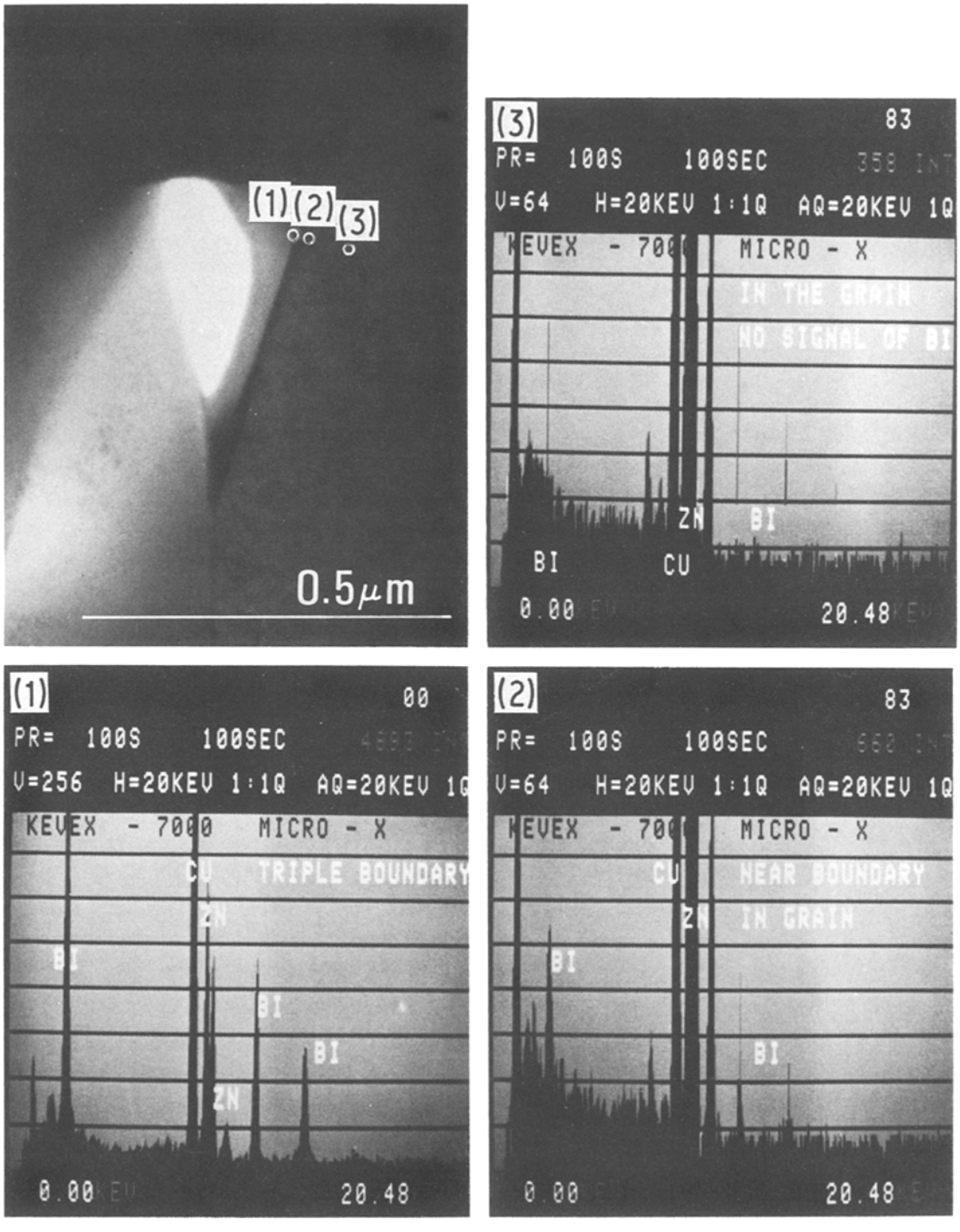

Figure 9 STEM analysis indicating a bismuth signal in a ZnO grain near a Bi_2O_3/ZnO grain boundary. Traces refer to Regions (1), (2) and (3) in the micrograph.

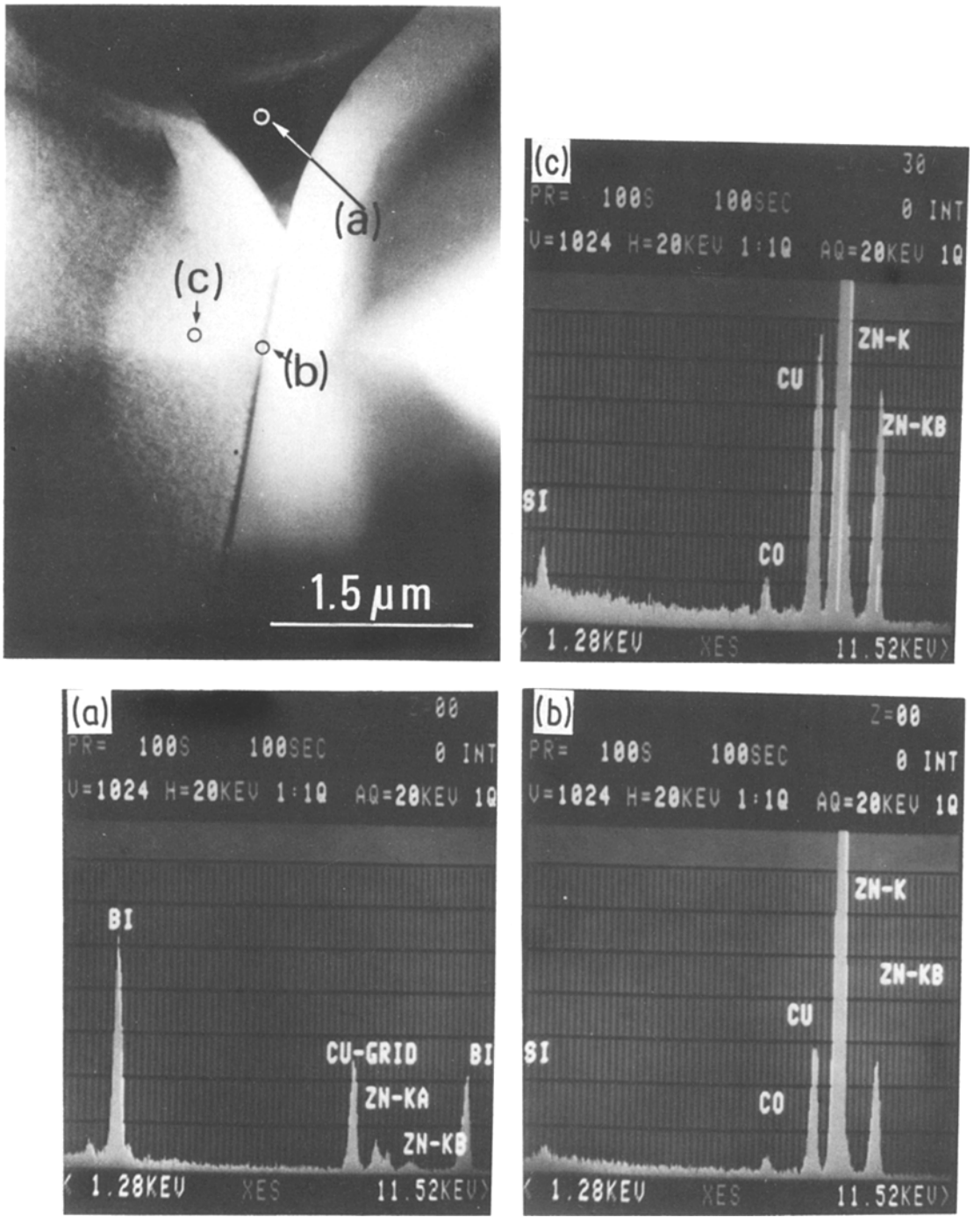

Figure 10 STEM analysis indicating no bismuth signal at a ZnO/ZnO grain boundary. Traces refer to Regions (a), (b) and (c) in the micrograph.

necessary for ZnO grains to be covered with a Bi_2O_3 layer. As is well known, the existence of a potential barrier is needed to cause the non-linear characteristics. The potential barrier is considered to originate from two factors at least. They are a disordered layer of 1 to 2 nm in width, and a distribution of additives at the ZnO/ZnO grain boundary.

We assume that Bi_2O_3 plays the part of distributing additives throughout the ZnO/ZnO grain boundaries, besides promoting the sintering of ZnO.

The conclusions obtained from this investigation will be helpful for considering the conduction mechanism and degradation mechanism of a zinc oxide varistor.

References

1. M. MATSUOKA, *Jpn. J. Appl. Phys.* **10** (1971) 736.
2. W. G. MORRIS, *J. Amer. Ceram. Soc.* **56** (1973) 360.
3. L. M. LEVINSON and H. R. PHILLIPP, *J. Appl. Phys.* **46** (1975) 1332.
4. M. INADA, *Jpn. J. Appl. Phys.* **17** (1978) 673.
5. J. WONG and W. G. MORRIS, *Amer. Ceram. Bull.* **53** (1976) 816.
6. W. G. MORRIS, *J. Vac. Sci. Technol.* **13** (1976) 926.
7. J. BERNASCONI, H. P. KLEIN, B. KNECHT and S. STRÄSSLER, *J. Electronic Mater.* **5** (1976) 473.
8. J. BERNASCONI, S. STRÄSSLER, B. KNECHT, H. P. KLEIN and A. MENTN, *Solid State Commun.* **21** (1977) 867.
9. P. R. EMTAGE, *J. Appl. Phys.* **48** (1977) 4372.
10. G. D. MAHAN, *ibid.* **50** (1979) 2799.
11. H. R. PHILLIPP and L. M. LEVINSON, *ibid.* **50** (1979) 383.
12. K. EDA, *ibid.* **49** (1978) 2964.
13. D. R. CLARKE, *ibid.* **49** (1978) 2407.
14. W. D. KINGERY, J. B. VAN DER SANDE and T. MITAMURA, *J. Amer. Ceram. Soc.* **62** (1979) 221.
15. YET-MINT CHIANG and W. D. KINGERY, *J. Appl. Phys.* **53** (1982) 1765.
16. R. SINCLAIR, R. GRONSKY and G. THOMAS, *Acta Metall.* **24** (1976) 789.
17. A. ZAV'YALOVA and IMAMOV, *Soviet Phys. Cryst.* **13** (1968) 37.

Received 2 November
and accepted 28 November 1984